

# PHOTOMASK

BACUS—The international technical group of SPIE dedicated to the advancement of photomask technology.

Best Paper Award - SPIE Photomask Japan 2015

## Pattern inspection of etched multilayer EUV mask

Susumu Iida, Ryoichi Hirano, Tsuyoshi Amano, and Hidehiro Watanabe,  
EUVL Infrastructure Development Center, Inc., 16-1 Onogawa, Tsukuba-shi,  
Ibaraki-ken, 305-8569, Japan

### ABSTRACT

Patterned mask inspection for an etched multilayer (ML) EUV mask was investigated. In order to optimize the mask structure from the standpoint of not only a pattern inspection by using a projection electron microscope (PEM), but also by considering the other fabrication processes using electron beam (EB) techniques such as CD metrology and mask repair, we employed a conductive layer between the ML and substrate. By measuring the secondary electron emission coefficients (SEECs) of the candidate materials for conductive layer, we evaluated the image contrast and the influence of charging effect. In the cases of 40-pair-ML, 16 nm sized extrusion and intrusion defects were found to be detectable more than 10 sigma in hp 44 nm, 40 nm, and 32 nm line and space (L/S) patterns. Reducing 40-pair-ML to 20-pair-ML degraded the image contrast and the defect detectability. However, by selecting  $B_4C$  as a conductive layer, 16 nm sized defects remained detectable. A double layer structure with 2.5-nm-thick  $B_4C$  on metal film used as a conductive layer was found to have sufficient conductivity and also was found to be free from the surface charging effect and influence of native oxide.

### 1. Introduction

Extremely Ultraviolet Lithography (EUVL) is the most advanced lithographic technology to fabricate 1x nm node devices. Pattern size shrinkage to near 10 nm requires an exposure tool with a higher numerical aperture (NA); and the high NA leads to an increase in the chief ray angle (CRA) of EUV light as shown in Fig. 1 (a).<sup>1</sup> As a result, mask 3D effect, such as shadowing effect, becomes larger with a conventional stacked absorber-type EUV mask structure (Fig. 1 (b)).<sup>2</sup> and thus, the lithography process margin decreases. Recently, T. Kamo et al. proposed that the binary etched multilayer (ML) mask is very effective to overcome this issue as shown in Fig. 1 (c).<sup>3-6</sup> Moreover, G. J. Kim et al. also confirmed this observation by numerical analysis.<sup>7-8</sup> However, mask structure should be taken into account when dealing with the mask fabrication processes such as patterned mask inspection.

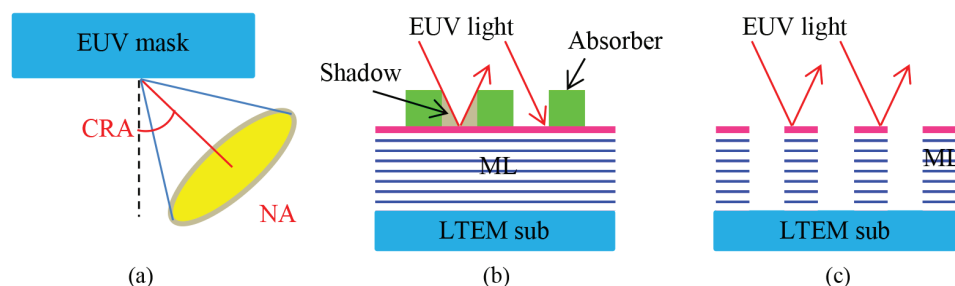


Figure 1. Schematic explanations of: (a) relationship between CRA and high-NA exposure, (b) shadowing effect of conventional EUV mask, and (c) etched ML EUV mask.

BACUS

N • E • W • S

SEPTEMBER 2015  
VOLUME 31, ISSUE 9

TAKE A LOOK  
INSIDE:

INDUSTRY BRIEFS  
— see page 11

CALENDAR  
For a list of meetings  
— see page 12

SPIE.

9658-47

# EDITORIAL

## Kudos to the mask maker

**Thomas Struck**, Infineon Technologies AG

Photomasks Forever! With these words, my colleague Hayashi-san closed his report from this year's 22nd Photomask Japan (PMJ 2015). Considering the global Photomask market, there are very advanced technology needs requiring everything that is physically feasible. On the one hand, only a handful of companies are using the most advanced technology nodes. On the other hand, there is still a large demand for mature Photomasks, which are the source for highly profitable semiconductor devices. Even if manufacturing of high quality, mature masks is no longer technically challenging, their on-time availability at a reasonable price is a key element in the success of the semiconductor product. The typical Photomask user at the wafer fab wants to keep life simple: A Photomask is ordered and just has "to be there" when needed.

According to VLSI Research/Semi Markets Reports, the worldwide demand for mature Photomasks will remain high in the future:

The latest VLSI Research analysis shows that approximately 170,000 pcs. of reticles were delivered for technology nodes  $\geq 350\text{nm}$  in 2014.

In terms of units, 130nm is still the most populated node (116,000 pcs. in 2014).

The current demand for all nodes  $\geq 90\text{nm}$  is 475,000 pcs. per year.

VLSI forecasts just a small drop of about 1.8% from today's 514,000 pcs. down to 504,000 pcs. in the technology nodes 500nm – 45nm by 2018.

The stable, high demand for mature Photomasks does not mean that there is no movement within this business. Actually, there is a lot of action.

Typically the products in the mature technology nodes are dedicated, customized for their applications and have long lifecycles. 10 years and more is common, for instance, for highly reliable automotive applications. Over the lifecycle of a certain semiconductor product, the customer expects continuous cost reduction measures to be implemented. Hence the whole supply chain, and the Photomask maker within it, is forced to reduce costs without any compromise in quality. The typical mature Photomask manufacturing company is a profit-driven sustainable venture. Within an environment where tools are typically fully depreciated and prices for raw materials are increasing, it is an on-going challenge for mask makers to maintain positive margins. As a consequence, even high-yielding and optimized processes have to be further improved to increase efficiency year on year. Profound know how, experience and commitment are the key for continuous improvement. I know mask houses that are fully operated by just a handful of engineers, who act as managers at the same time together with a dozen operators and technicians. Each staff member is highly motivated and responsible for a broad range of tasks.

Today the majority of mature Photomasks are manufactured using I-line Laser writers. These tools are often older than 15 years and are still reliable workhorses in the mature Photomask world. Most of the tools are no longer supported by the original manufacturer and the supply of spare parts is becoming more and more challenging. Just try to imagine a situation where the computer for 20-year old equipment breaks down and needs to be replaced in an integrated IT environment.

Users of mature Photomasks are continuously pushing for lower prices. Content reduction and process unifications are common and useful options for achieving a better cost basis. However, content reduction measures require process changes that lead to qualification efforts at the wafer fabs. In any case, no compromise in quality is allowed: Any changes made have to be proven to provide an equal or better result on wafer even if they were initiated for the sake of cost reduction. Furthermore, the Photomask users at the wafer fabs do not like change requests at all. Their resources are – of course – limited as well and they prefer not to have effort with evaluations and qualifications for things that just have "to be there". However, if the business case is ultimately positive, changes and qualifications will be supported.

In conclusion, the semiconductor industry benefits from Photomask makers who never stop improving even mature processes and therefore continuously make the whole manufacturing chain more efficient. Photomasks Forever!



N • E • W • S

BACUS News is published monthly by SPIE for BACUS, the international technical group of SPIE dedicated to the advancement of photomask technology.

**Managing Editor/Graphics** Linda DeLano

**Advertising** Lara Miles

**BACUS Technical Group Manager** Pat Wight

### ■ 2015 BACUS Steering Committee ■

#### President

Paul W. Ackmann, *GLOBALFOUNDRIES Inc.*

#### Vice-President

Jim N. Wiley, *ASML US, Inc.*

#### Secretary

Larry S. Zurbrick, *Keysight Technologies, Inc.*

#### Newsletter Editor

Artur Balasinski, *Cypress Semiconductor Corp.*

#### 2015 Annual Photomask Conference Chairs

Naoya Hayashi, *Dai Nippon Printing Co., Ltd.*

Bryan S. Kasprovicz, *Photonics, Inc.*

#### International Chair

Uwe F. W. Behringer, *UBC Microelectronics*

#### Education Chair

Artur Balasinski, *Cypress Semiconductor Corp.*

#### Members at Large

Frank E. Abboud, *Intel Corp.*

Paul C. Allen, *Toppan Photomasks, Inc.*

Michael D. Archuleta, *RAVE LLC*

Peter D. Buck, *Mentor Graphics Corp.*

Brian Cha, *Samsung*

Thomas B. Faure, *GLOBALFOUNDRIES Inc.*

Brian J. Grenon, *Grenon Consulting*

Jon Haines, *Micron Technology Inc.*

Mark T. Jee, *HOYA Corp, USA*

Patrick M. Martin, *Applied Materials, Inc.*

M. Warren Montgomery, *SUNY, The College of Nanoscale Science and Engineering*

Wilbert Odisho, *KLA-Tencor Corp.*

Jan Hendrik Peters, *Carl Zeiss SMS GmbH*

Michael T. Postek, *National Institute of Standards and Technology*

Abbas Rastegar, *SEMATECH North*

Douglas J. Resnick, *Canon Nanotechnologies, Inc.*

Thomas Struck, *Infineon Technologies AG*

Bala Thumma, *Synopsys, Inc.*

Jacek K. Tyminski, *Nikon Research Corp. of America (NRCA)*

Michael Watt, *Shin-Etsu MicroSi, Inc.*

## SPIE.

P.O. Box 10, Bellingham, WA 98227-0010 USA

Tel: +1 360 676 3290

Fax: +1 360 647 1445

www.SPIE.org

help@spie.org

©2015

All rights reserved.

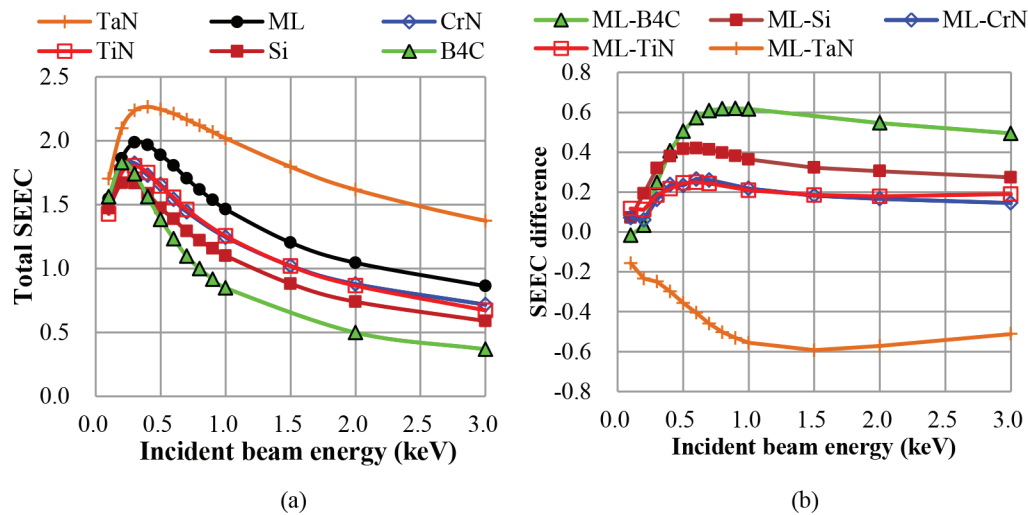


Figure 2. (a) Experimentally obtained SEECs of 100-nm-thick TaN, CrN, TiN, Si, B<sub>4</sub>C films, and Ru capped ML; and (b) their experimental SEEC difference (which was calculated by subtracting SEECs of these thin films from that of the Ru capped ML), as functions of incident beam energy. All the materials were measured in as-is conditions.

tion,<sup>9-13</sup> critical dimension measurement (CD metrology),<sup>14-15</sup> mask repair,<sup>16-17</sup> and cleaning.<sup>18</sup> K. Takai et al. reported that the reduction of ML stack down to 20 pairs effectively avoided the collapse of the lines by the cleaning process.<sup>19</sup> However, patterned mask inspection, CD metrology, and repair of this mask structure continue to pose challenges that need to be addressed. In these processes, electron beam (EB) techniques are often used, therefore, charging effects tend to cause some degradation of process accuracy. K. Takai et al. also reported that a conductive layer between SiO<sub>2</sub> substrate (or some low temperature expansion material (LTEM)) and ML was effective to avoid an electrical floating of the EUV mask inside a black border of etched ML. With this approach, the EB image quality of the mask was effectively improved.<sup>20</sup> As a result, the repeatability of metrology and the sensitivity of inspection for this type of EUV mask were also improved.<sup>20</sup> However, the optimization of material and structure of the conductive layer is critical, because this issue should be studied with taking into account the conductivity, durability for cleaning, oxidation, roughness, etching selectivity of the material, and the impact on the image contrast. We have learned that the image contrast is determined by the secondary electron emission coefficients (SEECs) of materials that EUV mask is composed of, and by the geometries involved. They also influence the defect detection sensitivity of a projection electron microscope (PEM) inspection system.<sup>21-24</sup> The PEM has an advantage of its much higher throughput than what is achievable in the case of conventional scanning electron microscope (SEM) type inspection system.<sup>9,11-13,21-25</sup>

That is because PEM probes a sample target with areal illumination, whereas SEM probes a sample with a spot beam. In this paper, we investigated the defect detectability of etched-ML-EUV-mask, and we propose a better and more feasible structure, which would improve the processing accuracy in working with EB systems.

## 2. Experimental

Candidate materials to serve as the conductive layers were selected among the familiar materials used in photomasks. TaN, Ru, CrN, TiN, Si are materials commonly used in EUV and conventional photomasks. B<sub>4</sub>C is also widely studied as an inter-diffusion barrier between Mo and Si for EUV reflective ML mirrors<sup>26</sup>, and as

a capping layer of the ML.<sup>27</sup> In order to evaluate the PEM image contrast of an L/S pattern, the SEECs of these materials with 100 nm thickness deposited on quartz substrates were measured using a specially designed scanning Auger microscope (SAM).<sup>28</sup> It should be noted that the obtained data were measured in as-is (as-deposited) conditions, with their native oxide films on their surface, in order to demonstrate the actual mask surface condition. The electrical resistivities of these films were measured by a four-point probe method with 0.3 mm spacings between the neighboring probes. In order to evaluate the defect detection sensitivity of a PEM inspection system, simulated PEM images were obtained using a CHARIOT Monte Carlo software (Abeam Technologies, Inc.).<sup>29</sup> The simulated PEM images take into account the characteristics of electron imaging optics (EOs), such as their aberrations, electron transmittance, and aperture stops, because these images are obtained at a conjugate image plane of the real application.<sup>25</sup> The pixel size of the image detector was 16 nm x 16 nm. A detailed method of simulated PEM image acquisition is described elsewhere.<sup>25</sup> In order to improve the reliability of the simulation results, the SEECs of the utilized materials were employed for the calibration of the simulation results. The difference between the simulated PEM image with defects and that without defects is defined as difference image. In order to define the sensitivity of defect detection, we identified the signal intensity in the difference image with more than 10 times the intensity of the standard deviation of the background intensity levels as a defect (10  $\sigma$ ). Image processing operations were applied to the simulated image to enhance the detect signal intensities.<sup>22,30</sup> The image contrast of L/S pattern is expressed as a modulation transfer function (MTF), defined as {(maximum value – minimum value) / (maximum value + minimum value)}

## 3. Results and Discussion

### 3.1 Analysis of the SEECs of utilized materials and their impacts on PEM image contrast

Figure 2 (a) shows the experimentally obtained SEECs of TaN, CrN, TiN, Si, B<sub>4</sub>C films, and Ru capped ML. The SEEC curves of CrN and TiN are almost identical; and the overall SEECs of

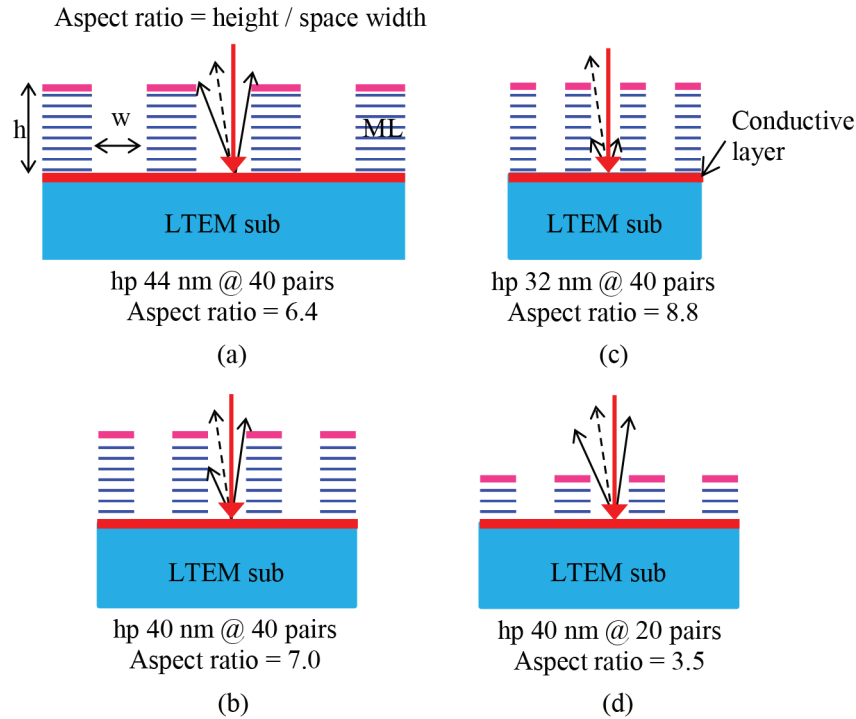


Figure 3. Schematic illustrations of SEs from the bottom of the etched ML mask with hp (a) 44 nm, (b) 40 nm, and (c) 32 nm L/S pattern in 40-pair-ML, and (d) 40 nm L/S pattern in 20-pair-ML. The aspect ratios of the L/S patterns are 6.4, 7.0, 8.8, and 3.5, respectively.

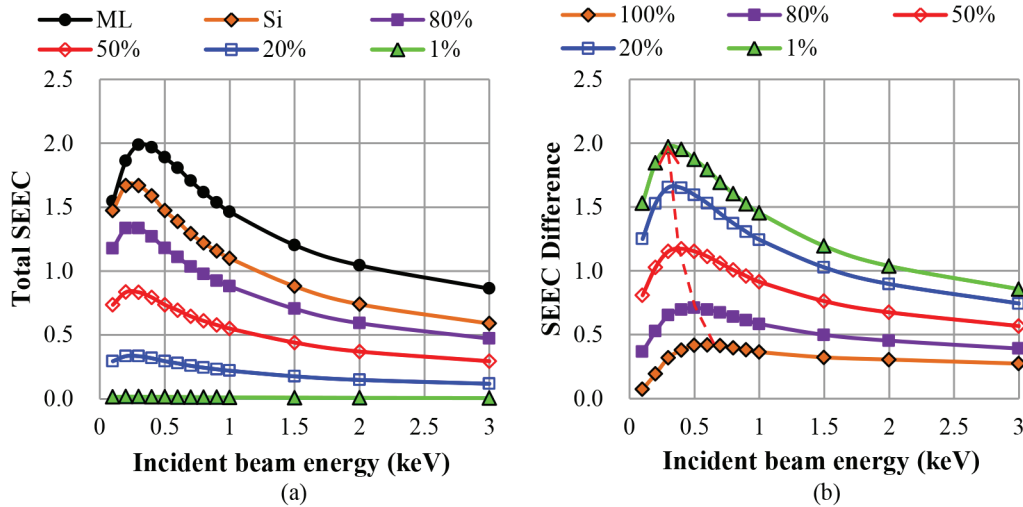


Figure 4. Apparent (a) SEEC and (b) SEEC difference change of high aspect ratio patterns on the Si layer.

B<sub>4</sub>C is the lowest among all these materials. These results make sense because the SEEC increases with the atomic number Z in general.<sup>31</sup> We have learned that the SEEC difference between lines and spaces determine the gray level difference of the captured images corresponding to the material contrasts.<sup>22,24</sup> As shown in Fig. 2 (b), the SEEC difference between ML and B<sub>4</sub>C turns out to be the largest. In the case of TaN, the SEEC difference shows a negative value because the SEECs of TaN is larger than those of ML. This result indicates that the combination of Ru capped ML and TaN exhibits the image contrast reversal as compared with

the other materials. The image contrast is also affected by the sample geometry. Especially for the etched ML mask, the aspect ratio of L/S pattern is considerably high, as shown in Fig. 3. The secondary electrons (SEs) generated from the bottom of the space are blocked by the sidewalls of the lines. Therefore, the SE signals from the space decrease as the aspect ratio becomes high.<sup>13,22,24,32</sup> Hence, this effect enhances the L/S pattern image contrast when the SEEC of the space material (conductive layer) is lower than that of ML.

Figure 4 shows the apparent SEEC and SEEC difference change

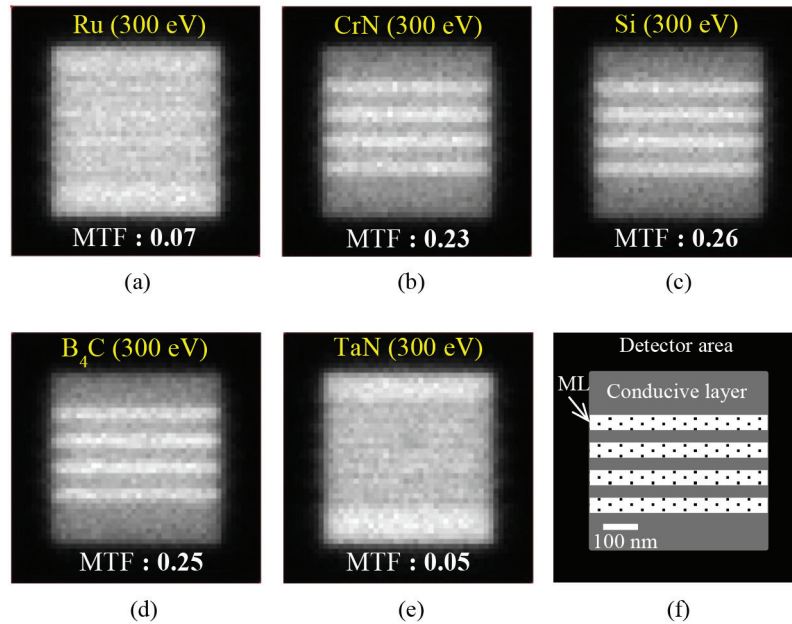


Figure 5. Simulated PEM image of etched 40-pair-ML EUV mask with hp 40 nm L/S pattern on the conductive layers of: (a) Ru, (b) CrN or TiN, (c) Si, (d) B<sub>4</sub>C, (e) TaN, and (f) their schematic illustration. Incident beam energy and MTF of L/S pattern are shown on the upper and lower parts of the image.

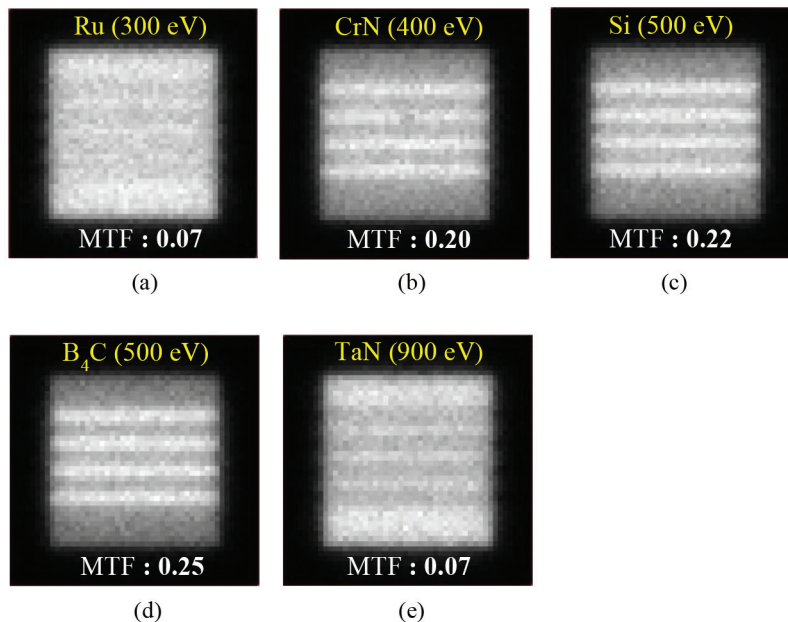


Figure 6. Simulated PEM image of etched 20-pair-ML EUV mask with hp 40 nm L/S pattern on the conductive layers of: (a) Ru, (b) CrN or TiN, (c) Si, (d) B<sub>4</sub>C, and (e) TaN. Incident beam energy and MTF of L/S pattern are shown on the upper and lower parts of the image.

of high aspect ratio pattern on Si layer. SEEC itself is one of the physical constants. However, a decrease in the SE signals from the bottom of the space can be considered as an apparent SEEC decrease for a better understanding of the phenomenon. As the percentage of the SE signals from the bottom decreases, the apparent SEEC becomes low as shown in Fig. 4 (a); while the apparent SEEC difference between ML and Si increase, and the

peak of the curve is shifted to the lower incident beam energy as shown in Fig. 4 (b). These results indicate that as the aspect ratio becomes high, the optimal incident beam energy to obtain the highest image contrast becomes low. Furthermore, when the SE signal from the bottom is extremely low (1%), the SEEC difference curve becomes identical to the SEEC curve of ML. As a result, the optimal condition is determined by the peak of the ML. This result



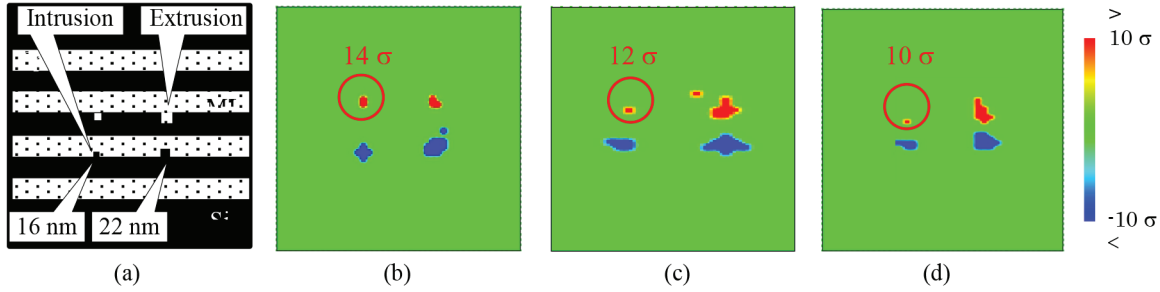


Figure 7. (a) Top view of the schematic illustration of etched 40-pair-ML EUV mask with defects, and difference images of (b) hp 44 nm, (c) hp 40 nm, and (d) hp 32 nm L/S patterns on the conductive layer of Si.

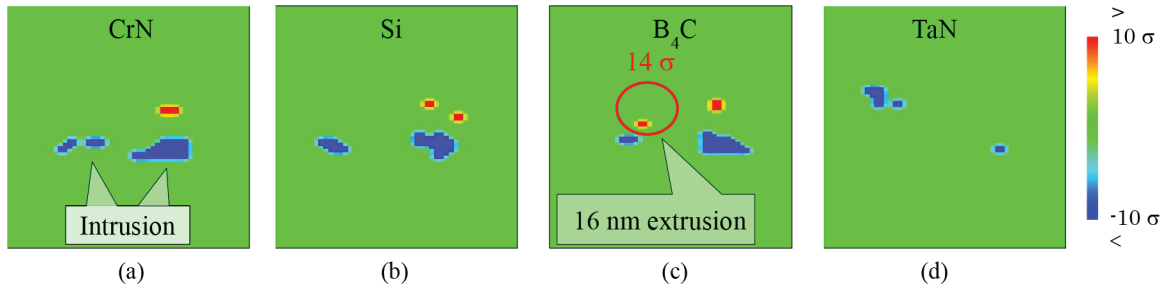


Figure 8. Difference images using etched 20-pair-ML EUV mask with hp 40 nm L/S pattern on the conductive layers of: (a) CrN or TiN, (b) Si, (c) B<sub>4</sub>C, and (d) TaN.

is in good agreement with our previous work for the investigation of the optimal incident beam energy to detect the small intrusion defect.<sup>22,24</sup> In order to confirm the impact of the conductive layer on the image contrast, simulated PEM images were obtained using a sample structure with hp 40 nm L/S pattern in 40-pair-ML on various conductive layers as shown in Fig. 5. Incident beam energy of 300 eV creates the most sensitive condition for defect detection in this sample geometry. In the case of Ru, the L/S pattern is hardly identifiable in spite of the high aspect ratio of 7.0 because their material contrast between Ru capped ML and Ru conductive layer is very low.<sup>23</sup> Moreover, the MTF of the TaN sample is lower than that of the Ru one because the higher SEEC of TaN cancels out the effect of a high aspect ratio. On the other hand, by reducing 40-pair-ML to 20-pair-ML, the MTF value of TaN sample increases; and the contrast of L/S pattern is reversed as compared with the CrN, Si, and B<sub>4</sub>C sample as shown in Fig. 6. These image contrasts correspond to their material contrasts derived from the SEEC curves as shown in Fig. 2. Furthermore, the MTF values of Si and B<sub>4</sub>C show a significant difference for the case with 20-pair-ML (0.22 and 0.25, respectively), whereas the values for the case with 40-pair-ML are about the same (0.26 and 0.25, respectively). These results indicate that the conductive layer underlying 20-pair-ML has a greater impact on the EB image contrast than in the case of 40-pair-ML; and that the B<sub>4</sub>C sample has the highest image contrast of the L/S pattern. It is also noted that the optimal incident beam energy for defect detection in the geometry of 20-pair-ML is higher than that of the 40-pair-ML, due to an increase in the percentage of the detectable SEs from the conductive layer as shown in Fig. 4 (b).

### 3.2 Investigation of the impact of aspect ratio and conductive layer on defect detectability

In order to investigate the impact of the aspect ratio and conductive layer on the defect detectability of a PEM inspection system

for etched ML EUV mask, a die-to-die inspection is demonstrated using simulated PEM images with and without defects. Fig. 7 shows the difference images for the cases of 40-pair-ML on Si layer. A set of extrusion and intrusion defects with 22 nm and 16 nm sizes are detected more than 10  $\sigma$  in all the cases of hp 44 nm, 40 nm, and 32 nm L/S pattern. As shown in Figs. 3 (a), (b), and (c), their aspect ratios are 6.4, 7.0, and 8.8, respectively. The illumination and the imaging systems used for this simulation are designed for hp 64 nm L/S pattern (hp 16 nm on wafer). Therefore the spatial resolution is not sufficient for smaller hp L/S patterns such as less than hp 40 nm (hp 10 nm on wafer). Thus, the defect detection sensitivity degrades along with the pattern size shrink in spite of the increase of aspect ratio. We have learned that the spatial resolution has a great impact on the defect detectability especially for small defects.<sup>13</sup> In order to increase the detectability, the spatial resolution needs to be improved, and we are now developing a new PEM inspection system designed for 11 nm node.<sup>33</sup>

Fig. 8 shows the difference images for the cases of 20-pair-ML with hp 40 nm L/S pattern on various conduction layer. By reducing 40-pair-ML to 20-pair-ML, 16 nm sized extrusion defect on Si layer becomes undetectable. Only in the case of B<sub>4</sub>C sample, 16 nm sized extrusion defects are detected more than 10  $\sigma$ . These results indicate that the selection of a conductive layer with higher material contrast is critical for high sensitive pattern inspection of etched 20-pair-ML EUV mask. In order to confirm the threshold level for defect detection, the difference images with various threshold levels are shown in Fig. 9. In the case of 5  $\sigma$ , 16 nm extrusion defect is detected even on Si, but some false defects are also observed in all samples. As increasing the threshold, the false defects decrease, and then, in the case of 10  $\sigma$ , 16 nm sized extrusion defect are detected without any false defects on B<sub>4</sub>C sample. This result indicates that 10  $\sigma$  is the required condition for inspection without false defects.

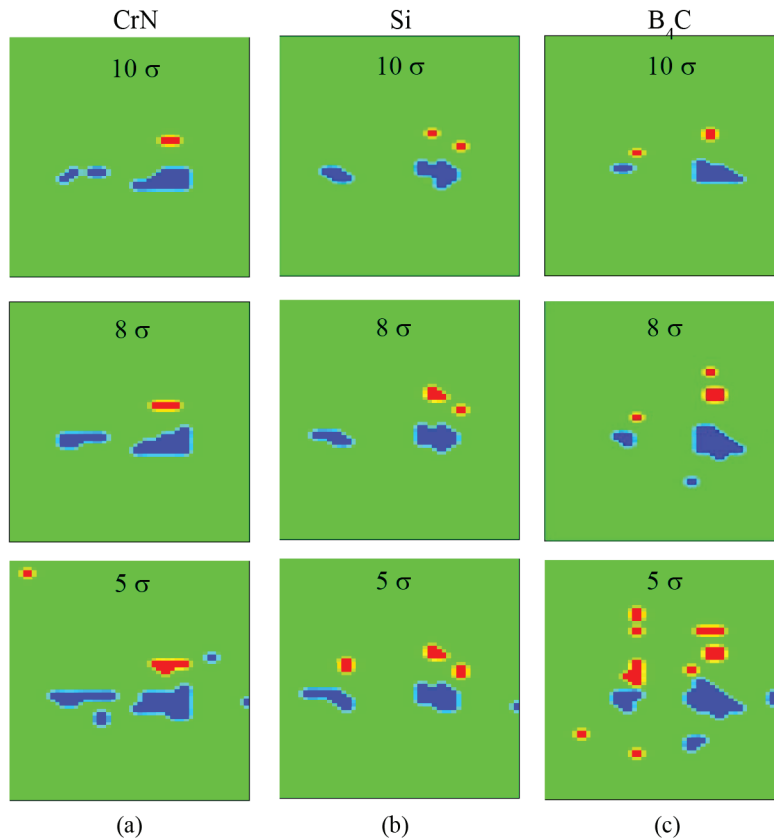


Figure 9. Difference images using etched 20-pair-ML EUV mask with hp 40 nm L/S pattern on the conductive layers of: (a) CrN or TiN, (b) Si, and (c) B<sub>4</sub>C with various threshold levels.

### 3.3 Analysis of electrical conductivity and charging effect of the candidate materials

In order to investigate electrical conductivity and surface charging effect of the candidate materials, electrical resistivity and the dependence of beam probe current on the SEEC are evaluated. Table 1 shows the resistivity of the candidate materials with various structures. TiN, CrN, and TaN have good conductivities. In the case of Si, the resistivity of p- or n-type crystal Si are known as  $1.0 - 1.0 \times 10^{-2} \Omega\text{cm}$ . However, crystal layers are hardly grown on non-crystalline substrates such as quartz and LTEM. Especially for the case of sputtered films, amorphous Si with high resistivity tends to be deposited. On the other hand, B<sub>4</sub>C with 100 nm has a comparatively good conductivity, but the electric resistance of 5-nm-thick B<sub>4</sub>C film on SiO<sub>2</sub> substrate goes up to an unmeasurable level. From the standpoint of EB repair technique, a resistivity should be low as possible to demonstrate the precise repair process.<sup>16-17</sup> These results show that Si conductive layer has a technical problem with depositions on to photomask substrates,

and a B<sub>4</sub>C film does not seem to be sufficiently conductive to maximize the accuracy of the repair process, CD metrology, and the sensitivity of pattern inspection. In order to maximize the effect of low SEEC and electrical conductivity, a conductive layer with double layer structure with 2.5-nm-thick B<sub>4</sub>C on metal film is proposed. The resistivity of this type of conductive layer is better than those of TiN, CrN, and TaN. In order to reconfirm the conductivity, and investigate the effect of surface charging when the electron beam is irradiated, the dependence of the beam current on the SEEC changes were examined for the three types of B<sub>4</sub>C samples as shown in Fig. 10. The SEECs of 100 nm-thick-B<sub>4</sub>C film and 2.5-nm-thick B<sub>4</sub>C on metal film remain almost constant as the incident electron beam current increases. On the other hand, the SEEC of the 5-nm-thick B<sub>4</sub>C film shows a significant decrease with the increasing beam current, because the emitted SEs return back to the sample surface due to the strong positive charges involved as shown in Fig. 11.<sup>24,34-35</sup> When the B<sub>4</sub>C film is sufficiently thick, the injected electrons or generated holes can be discharged through

Table 1. Electrical resistivity of the candidate layers ( $\Omega\text{cm}$ ).

TiN	CrN	TaN	Doped crystal -Si	a-Si	B <sub>4</sub> C	B <sub>4</sub> C (5 nm)	2.5-nm-B <sub>4</sub> C on metal film
$1.0 \times 10^{-4}$	$1.4 \times 10^{-4}$	$2.3 \times 10^{-4}$	$\sim 1.0$	Unmeasurable	23.3	Unmeasurable	$< 5.4 \times 10^{-5}$

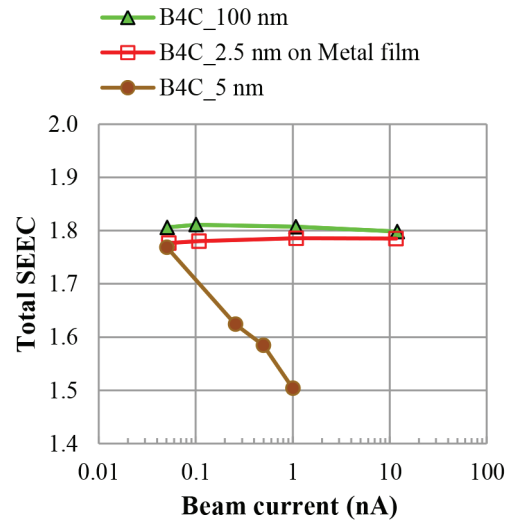


Figure 10. Experimentally obtained SEECs of 100 nm-thick  $B_4C$  film, 2.5-nm-thick  $B_4C$  on metal film, and 5-nm-thick  $B_4C$  film as functions of primary electron current with a beam energy of 200 eV (the maximum values of their yield curves). Diameter of the focused incident beam was estimated to be  $\sim 1.2 \mu\text{m}$  at 2 nA with 200 eV.

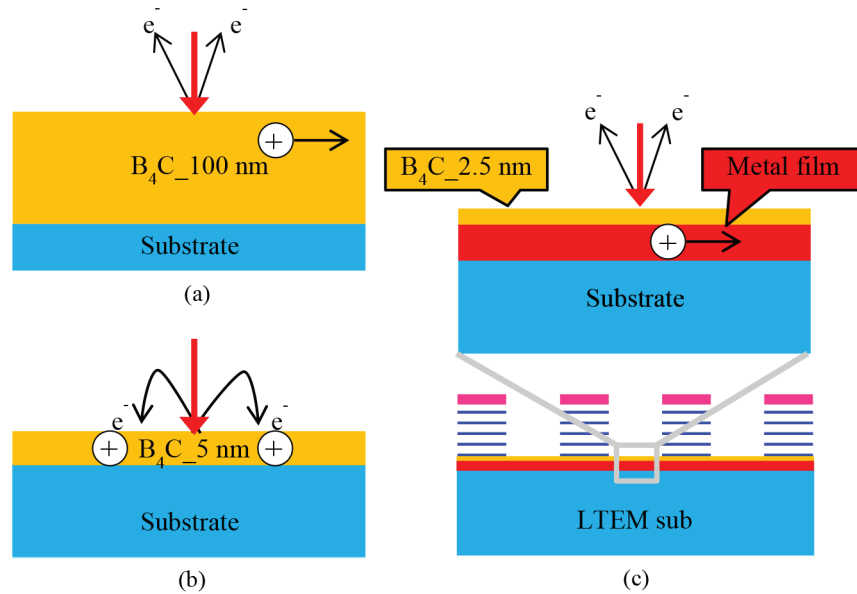


Figure 11. Schematic explanations of the charging and discharging effects for the samples of: (a) 100-nm-thick  $B_4C$  film, (b) 2.5-nm-thick  $B_4C$  on metal film, and (c) 5-nm-thick  $B_4C$  film.

the thick  $B_4C$  film. However, these charges are stored in the thin  $B_4C$  film due to its extreme high resistance. On the other hand, in the case of the double layer structure, the charges are discharged along with the underlying metal film. We have already reported that the SEEC of the nondoped Si layer with the resistivity of  $> 1000 \Omega\text{cm}$  shows a similar decrease along with the increasing beam current, whereas the SEECs of the Ru-capped ML remain almost constant.<sup>24</sup> Moreover, the lateral and vertical conductivities of Ru-capped ML is empirically known to be sufficiently high to avoid any charging effect in spite of 4-nm-thick-sputtered Si layers being included.<sup>20</sup> These results indicate that the charging effect attributed to the 2.5-nm-thick  $B_4C$  is negligibly small, and

the SE signal from the double structured conductive layer is not changed regardless of the electron dosage.

### 3.4 The “other” items to be taken into account in selecting the conductive layer

In order to select the conductive layer, the following “other” items to be taken into account are discussed: (I) influence of native oxide, (II) etching selectivity, and (III) additional phase defects.

- (I) If the native oxide is thicker than the conductive layer, patterns become electrically floating as shown in Fig. 12 (a-1). On the other hand, if the native oxide is thinner than the conductive layer, the native oxide does not affect the mask conductivity, but does affect the surface charging as



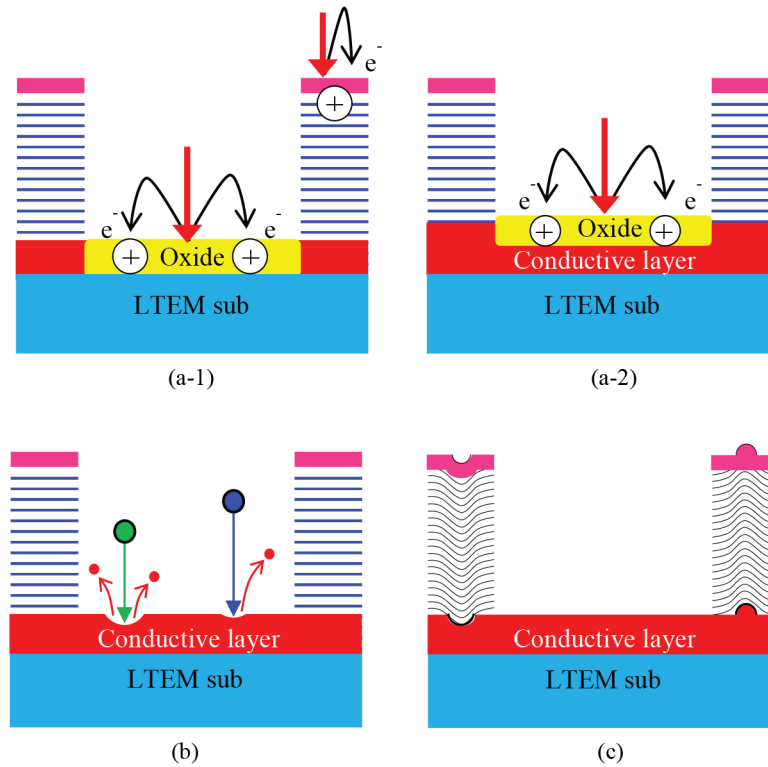


Figure 12. Schematic explanations of (a-1)-(a-2) influence of native oxide, (b) etching selectivity, and (c) phase defects.

shown in Fig. 12 (a-2). However, if the metal film is capped by the  $B_4C$ , the conductive layer is not affected by the native oxide.<sup>27</sup> Hence, the question of native oxide can be resolved by using the double-layer structure with 2.5-nm-thick  $B_4C$  on metal film.

- (II) The conductive layer should play a role of etch stop layer of a dry etch process. The ML is composed of Si and Mo, therefore, Si is not adequate for the conductive layer from the standpoint of etching selectivity as shown in Fig. 12 (b).  $B_4C$  is known as a very stable component and has strong chemical and mechanical resistance.<sup>27</sup> However, the etching selectivity against the ML should be confirmed, or the appropriate etching condition should be studied.
- (III) Additional phase defects derived from the conductive layer should be suppressed. The phase defect is one of the issues to be addressed on EUV mask.<sup>36-37</sup> Pit or bump defect on the mask substrate, and particles attached before and during the deposition process of ML are the origins of phase defects as shown in Fig. 12 (c). The influence of the conductive layer on the increase or decrease of phase defect should be investigated.

#### 4. Summary and Conclusion

Patterned mask inspection for an etched multilayer (ML) EUV mask was investigated. In order to optimize the mask structure from the standpoint of not only a pattern inspection using PEM, but also considering other fabrication processes using EB technique such as CD metrology and mask repair, we focus on a conductive layer between the ML and substrate. Candidate materials to serve as the

conductive layer were selected from the familiar materials used in photomasks such as TaN, Ru, CrN, TiN, Si and  $B_4C$ . By measuring the SEECs of the candidate materials for conductive layer, the combination of  $B_4C$  conductive layer and Ru capped ML was found to have the best pattern image contrast due to its highest SEEC difference. In the cases of 40-pair-ML, 16 nm sized extrusion and intrusion defects were found to be detectable more than 10  $\sigma$  in hp 44 nm, 40 nm, and 32 nm L/S pattern. Although by reducing 40-pair-ML to 20-pair-ML degraded the image contrast and the defect detectability, 16 nm sized defects remained detectable in the case of  $B_4C$  sample. In order to maximize the effect of low SEEC and electrical conductivity, a double-layer structured conductive layer with 2.5-nm-thick  $B_4C$  on metal film was proposed. This conductive layer was found to have sufficient conductivity ( $< 5.4 \times 10^{-5} \Omega\text{cm}$ ) and also was found to be free from the surface charging effect and influence of native oxide.

#### 5. Acknowledgement

The authors would like to thank T. Kamo, K. Takai, M. Naka, R. Yoshikawa, S. Kanamitsu, and T. Hirano of Toshiba Corporation for useful discussions. This work was supported by New Energy and Industrial Technology Development Organization (NEDO).

#### 6. References

- [1] B. Kneer, S. Migura, W. Kaiser, J. T. Neumann, and J. V. Schoot, "EUV lithography optics for sub-9nm resolution," *Proc. SPIE* **9422**, 94221G (2015).
- [2] J. T. Neumann, P. Gräupner, W. Kaiser, R. Garreis, and B. Geh, "Interactions of 3D mask effects and NA in EUV lithography," *Proc. SPIE* **8522**, 852211 (2012)

- [3] B. La Fontaine, A. R. Pawloski, Y. Deng, C. Chovino, L. Dieu, O. R. Wood II, and H. J. Levinson, "Architectural choices for EUV Lithography masks: patterned absorbers and patterned reflectors," **Proc. SPIE** **5374**, 300 (2004).
- [4] T. Schmoeller, J. K. Tyminski, J. Lewellen, and W. Demmerle, "The Impact of Mask Design on EUV Imaging," **Proc. SPIE** **7379**, 73792H (2009).
- [5] C. Chovino, L. Dieu, E. Johnstone, J. Reyes, B. M. La Fontaine, H. J. Levinson, and A. R. Pawloski "EUV Mask Making: An Approach Based on the Direct Patterning of the EUV Reflector," **Proc. SPIE** **5256**, 566 (2003).
- [6] K. Takai, T. Motokawa, K. Murano, T. Kamo, and N. Hayashi, "Patterning of EUVL binary etched multilayer mask," **Proc. SPIE** **8880**, 88802M (2013).
- [7] G. J. Kim, H. K. Oh, I. S. Kim, M. Yeung, and E. Barouch, "Etched multilayer mask is better than conventional absorber mask," **Proc. SPIE** **9256**, 92560R (2014).
- [8] G. J. Kim, M. Yeung, E. Barouch, and H. K. Oh, "Etched multilayer mask in EUV lithography for 16 nm node and below," **Proc. SPIE** **9256**, 92560Q (2014).
- [9] S. Yamaguchi, M. Naka, M. Kadowaki, T. Koike, T. Hirano, M. Itoh, Y. Yamazaki, K. Terao, M. Hatakeyama, K. Watanabe, H. Sobukawa, T. Murakami, K. Tsukamoto, T. Hayashi, N. Kimura, and N. Hayashi, "Performance of EBeyeM for EUV Mask Inspection," **Proc. SPIE** **8166**, 81662F (2011).
- [10] T. Shimomura, S. Narukawa, T. Abe, T. Takikawa, N. Hayashi, F. Wang, L. Ma, C. W. Lin, Y. Zhao, C. Kuan, and J. Jau, "Electron beam inspection of 16 nm HP node EUV masks," **Proc. SPIE** **8522**, 85220L (2012).
- [11] R. Hirano, H. Watanabe, S. Iida, T. Amano, T. Terasawa, M. Hatakeyama, and T. Murakami, "Development of extreme ultraviolet mask pattern inspection technology using projection electron beam optics," *J. Micro/Nanolith. MEMS MOEMS* **12**, 021003 (2013).
- [12] R. Hirano, S. Iida, T. Amano, T. Terasawa, H. Watanabe, M. Hatakeyama, T. Murakami, and K. Terao, "Patterned mask inspection technology with projection electron microscope technique on extreme ultraviolet masks," *J. Micro/Nanolith. MEMS MOEMS* **13**, 013009 (2014).
- [13] S. Iida, R. Hirano, T. Amano, and H. Watanabe, "Dependence of defect size and shape on detectability for EUV patterned mask inspection," **Proc. SPIE** **9422**, 942225 (2015).
- [14] Y. Nishiyama, H. Hakii, I. Yonekura, K. Tanaka, and Y. Kikuchi, "Influence of the charging effect on the precision of measuring EUV mask features," **Proc. SPIE** **7971**, 79710C (2011).
- [15] S. Babin, S. Borisov, H. Hakii, Y. Nishiyama, and I. Yonekura, "CD-Metrology of EUV Masks in the Presence of Charging: Measurement and Simulation," **Proc. SPIE** **8441**, 844108 (2012).
- [16] S. Kanamitsu, T. Hirano, and O. Suga, "Prospect of EUV mask repair technology using e-beam tool," **Proc. SPIE** **7823**, 782322 (2010).
- [17] S. Kanamitsu, K. Morishita, and T. Hirano, "Application of EB repair for high durable MoSi PSM," **Proc. SPIE** **9256**, 92560U (2014).
- [18] U. Dietze, P. Dress, T. Waehler, S. Singh, R. Jonckheere, and B. Baudemprez, "Effective EUVL mask cleaning technology solutions for mask manufacturing and in-fab mask maintenance," **Proc. SPIE** **7985**, 79850N (2011).
- [19] K. Takai, K. Murano, T. Kamo, Y. Morikawa, and N. Hayashi, "Capability of etched multilayer EUV mask fabrication," **Proc. SPIE** **9235**, 923515 (2014).
- [20] K. Takai, K. Murano, E. Yamanaka, S. Yamaguchi, M. Naka, T. Kamo, and N. Hayashi, "Improvement of EUVL mask structure with black border of etched multilayer," **Proc. SPIE** **8701**, 87010Y (2013).
- [21] S. Iida, T. Amano, R. Hirano, T. Terasawa, and H. Watanabe, "Identification of residual-type defect on extreme ultraviolet mask by projection electron microscope using Monte Carlo simulation," *J. Vac. Sci. Technol. B* **30**, 06F503 (2012).
- [22] S. Iida, T. Amano, R. Hirano, T. Terasawa, and H. Watanabe, "Extreme ultraviolet mask defect inspection with a half pitch 16-nm node using simulated projection electron microscope images," *J. Micro/Nanolith. MEMS-MOEMS* **12**, 023013 (2013).
- [23] S. Iida, T. Amano, R. Hirano, T. Terasawa, and H. Watanabe, "Impact of electron scattering in extreme ultraviolet reflective multilayer on electron image," *J. Vac. Sci. Technol. B* **31** (6), 06F601 (2013).
- [24] S. Iida, R. Hirano, T. Amano, and H. Watanabe, "Impact of B4C capping layer for extreme ultraviolet mask on the sensitivity of patterned mask inspection using a projection electron microscope," *J. Micro/Nanolith. MEMS-MOEMS* **13**, 043015 (2014).
- [25] S. Iida, R. Hirano, T. Terasawa, T. Amano, and H. Watanabe, "Analysis of image distortion on projection electron microscope image," *Jpn. J. Appl. Phys.* **53**, 116602 (2014).
- [26] S. Bajt, J. Alameda, T. Barbee Jr., W.M. Clift, J.A. Folta, B. Kaufmann, and E. Spiller, "Improved reflectance and stability of Mo/Si multilayers," *Opt. Eng.*, **41**, 1797 (2002).
- [27] I. Y. Jang, A. John, F. Goodwin, S. Y. Lee, B. G. Kim, S. S. Kim, C. U. Jeon, J. H. Kim, and Y. H. Jang, "Ruthenium (Ru) Peeling and Predicting Robustness of the Capping Layer Using Finite Element Method (FEM) Modeling," **Proc. SPIE** **9256**, 92560I (2014).
- [28] M. Kadowaki, A. Hamaguchi, H. Abe, Y. Yamazaki, S. Borisov, A. Ivanchikov, and S. Babin, "Investigation of factors causing difference between simulation and real SEM image," **Proc. SPIE** **7272**, 72723I (2009).
- [29] S. Babin, S. Borisov, A. Ivanchikov, and I. Ruzavin, "CHARIOT: software tool for modeling SEM signal and e-beam lithography," **Physics Procedia** **1**, 305 (2008).
- [30] H. Watanabe, R. Hirano, S. Iida, T. Amano, T. Terasawa, M. Hatakeyama, T. Murakami, S. Yoshikawa, and K. Terao, "EUV patterned mask inspection system using a projection electron microscope technique," **Proc. SPIE** **8880**, 88800U (2013).
- [31] Y. Lin and D. C. Joy, "A new examination of secondary electron yield data," *Surf. Interface Anal.*, **37**, 895 (2005).
- [32] D. Bizen, Y. Sohda, and H. Kazumi, "Dependence of Secondary-electron Yield on Aspect Ratio of Several Trench Patterns," **Proc. SPIE** **9050**, 90500K (2014).
- [33] R. Hirano, S. Iida, T. Amano, H. Watanabe, M. Hatakeyama, T. Murakami, S. Yoshikawa, K. Karimata and K. Terao, "Study of EUVL patterned mask inspection tool for half-pitch (hp) 16nm-11nm node," **Proc. SPIE** **9422**, 942224 (2015).
- [34] S. Aoyagi and K. Ura, "Initialization by erasing the surface potential of negatively charged insulators in scanning electron microscope (SEM) observation," *J. Electron Microsc.* **48**, 555 (1999).
- [35] M. Miyoshi and K. Ura, "Negative charging-up contrast formation of multilayered structures with a nonpenetrating electron beam in scanning-electron microscope," *J. Vac. Sci. Technol. B* **23**, 2763 (2005).
- [36] T. Amano, and T. Terasawa, "Propagation of surface topography of extreme ultraviolet blank substrate through multilayer and impact of phase defect structure on wafer image," *J. Micro/Nanolith. MEMS MOEMS* **12**, 033015 (2013).
- [37] T. Harada, Y. Tanaka, T. Watanabe, H. Kinoshita, Y. Usui, and T. Amano, "Phase defect characterization on an extreme-ultraviolet blank mask using microcoherent extreme-ultraviolet scatterometry microscope," *J. Vac. Sci. Technol. B* **31**, 06F605 (2013).



## Sponsorship Opportunities

Sign up now for the best sponsorship opportunities

### Photomask 2015 –

Contact: Lara Miles, Tel: +1 360 676 3290;  
laram@spie.org

### Advanced Lithography 2016 –

Contact: Lara Miles, Tel: +1 360 676 3290;  
laram@spie.org

## Advertise in the BACUS News!

The BACUS Newsletter is the premier publication serving the photomask industry. For information on how to advertise, contact:

Lara Miles  
Tel: +1 360 676 3290  
laram@spie.org

## BACUS Corporate Members

Acuphase Inc.  
American Coating Technologies LLC  
AMETEK Precitech, Inc.  
Berliner Glas KGaA Herbert Kubatz  
GmbH & Co.  
FUJIFILM Electronic Materials U.S.A., Inc.  
Gudeng Precision Industrial Co., Ltd.  
Halocarbon Products  
HamaTech APE GmbH & Co. KG  
Hitachi High Technologies America, Inc.  
JEOL USA Inc.  
Mentor Graphics Corp.  
Molecular Imprints, Inc.  
Panavision Federal Systems, LLC  
Profilocolore Srl  
Raytheon ELCAN Optical Technologies  
XYALIS

# Industry Briefs

## ■ Shin-Etsu Chemical to Build Photomask Blanks Plant in Japan

### Chemicals Technology, June 22, 2015

Shin-Etsu Chemical is planning to invest approximately JPY7bn (\$56m) to build a new photomask blanks plant in Echizen City, Fukui Prefecture, Japan. The company has already acquired land for the project and is expecting to commence operations by the end of 2016. The company's photomask blanks production capacity would increase by 20% from its present level. The new plant will be built to steadily capture the rapidly expanding demand for photomask blanks. In addition, the new plant will allow the company to have multiple photomask blanks production bases. The company commercialized photomask blanks in 2009 and started production at its Naoetsu Plant in Niigata Prefecture, Japan. Going forward, the company intends to double its present production capacity. The company plans to minimize business risks by having two production bases so that it will be able to fulfill its responsibility to supply products to customers even if a serious unexpected event such as a natural disaster occurs.

## ■ Semiconductor Market Worth \$332B in 2015

### Solid State Technology, July 28, 2015

The Global Semiconductor Market 2015 – 2020 research report forecasts revenues for key services across key geographies. The global semiconductor market is forecast to reach \$332bn across 2015, representing a 3.4 percent growth in comparison to \$316bn in 2014. This research forecasts that the market will grow at a 5-yr CAGR of 2.9 percent over 2015 to 2020, with the majority of growth being driven by mobile, automotive and industrial application markets. The consumer electronics and data processing application markets are expected to remain at the end of the growth spectrum with limited expectations for any innovative development to lead market demand. Top 20 global semiconductor industry players, by revenue, 2014 listed in this research include Intel, Samsung, Qualcomm, Micron, SK Hynix, Texas Instruments, Toshiba, Broadcom, TSMC, STM, MediaTek, Renesas, SanDisk, Infineon, NXP, Avago, AMD, Freescale, Sony, and NVIDIA.

The second research titled "Global and China Semiconductor Equipment Industry Report, 2014-2015, says in 2014, the global semiconductor equipment market size totaled USD38 billion, up 10.4 percent from 2013. It is predicted that in 2015 this figure will climb to USD40.5 billion, a rise of 6.7 percent from a year ago, and that the market size in 2016 will slump by 5.6 percent as compared to 2015. However, the possible shrinkage in 2016 might come from the following factors:

Firstly, following a peak in 2014, main electronic products such as smartphones and tablet and laptop PCs have stagnated or declined. This is particularly true of tablet PCs, which has presented a significant decline. On the other hand, equipment market delays being sluggish but will without doubt decline in 2016.

Secondly, due to the global deflation, prices for bulk commodity led by oil and iron ore plunged and would cause knock-on effect, which would in turn result in a fall in semiconductor equipment prices.

Thirdly, global economic recovery will probably come to a halt, with the US GDP dropping by 0.7 percent in 2015Q1. Moreover, China's GDP growth slowed obviously. Both countries constituted the major driving force of the global economy. The stimulatory effect of US QE began to fade away, and therefore the economy might go down.

In 2014, semiconductor equipment vendors made remarkable performance, with a substantial rise in operating profit, though their revenue did not increase. The merger of Applied Material and Tokyo Electron was rejected by the US Department of Commerce. In future, more of M&A plans may well be intervened by the government, after all, semiconductor equipment market is a highly concentrated market.

# Join the premier professional organization for mask makers and mask users!

## About the BACUS Group

Founded in 1980 by a group of chrome blank users wanting a single voice to interact with suppliers, BACUS has grown to become the largest and most widely known forum for the exchange of technical information of interest to photomask and reticle makers. BACUS joined SPIE in January of 1991 to expand the exchange of information with mask makers around the world.

The group sponsors an informative monthly meeting and newsletter, BACUS News. The BACUS annual Photomask Technology Symposium covers photomask technology, photomask processes, lithography, materials and resists, phase shift masks, inspection and repair, metrology, and quality and manufacturing management.

### Individual Membership Benefits include:

- Subscription to BACUS News (monthly)
- Eligibility to hold office on BACUS Steering Committee

[www.spie.org/bacushome](http://www.spie.org/bacushome)

### Corporate Membership Benefits include:

- 3-10 Voting Members in the SPIE General Membership, depending on tier level
- Subscription to BACUS News (monthly)
- One online SPIE Journal Subscription
- Listed as a Corporate Member in the BACUS Monthly Newsletter

[www.spie.org/bacushome](http://www.spie.org/bacushome)

## Calendar

### 2015



#### **SPIE Photomask Technology**

29 September-1 October 2015  
Monterey Marriott and  
Monterey Conference Center  
Monterey, California, USA  
[www.spie.org/pm](http://www.spie.org/pm)

*Co-located with*

**SPIE Scanning Microscopies**  
[www.spie.org/sg](http://www.spie.org/sg)

### 2016



#### **SPIE Advanced Lithography**

San Jose Convention Center  
and San Jose Marriott  
San Jose, California, USA  
[www.spie.org/al](http://www.spie.org/al)

*Abstracts Due 8 September*

SPIE is the international society for optics and photonics, an educational not-for-profit organization founded in 1955 to advance light-based technologies. The Society serves nearly 264,000 constituents from 166 countries, offering conferences, continuing education, books, journals, and a digital library in support of interdisciplinary information exchange, professional networking, and patent precedent. SPIE provided more than \$4 million in support of education and outreach programs in 2014. [www.spie.org](http://www.spie.org)

### **SPIE.**

*International Headquarters*

P.O. Box 10, Bellingham, WA 98227-0010 USA

Tel: +1 360 676 3290

Fax: +1 360 647 1445

[help@spie.org](mailto:help@spie.org) • [www.SPIE.org](http://www.SPIE.org)

*Shipping Address*

1000 20th St., Bellingham, WA 98225-6705 USA

### **Managed by SPIE Europe**

2 Alexandra Gate, Ffordd Pengam, Cardiff,  
CF24 2SA, UK

Tel: +44 29 2089 4747

Fax: +44 29 2089 4750

[spieeurope@spieeurope.org](mailto:spieeurope@spieeurope.org) • [www.spieeurope.org](http://www.spieeurope.org)

You are invited to submit events of interest for this calendar. Please send to [lindad@spie.org](mailto:lindad@spie.org); alternatively, email or fax to SPIE.